Journal of Materials Chemistry A

Accepted Manuscript

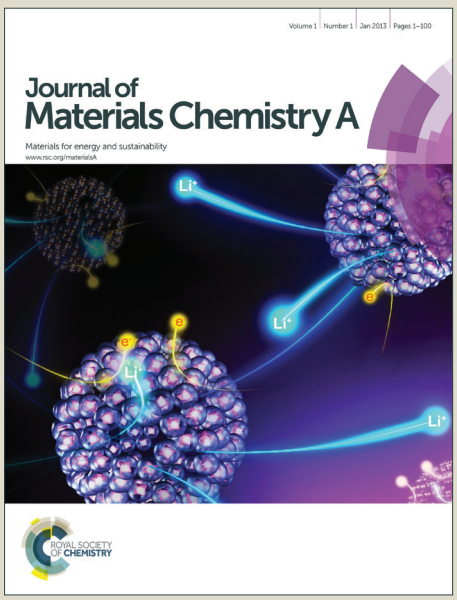

ROYAL SOCIETY OF CHEMISTRY

www.rsc.org/materialsA

Periodically Textured Metal Electrodes: Large-Area Fabrication, Characterization, Simulation, and Application as Efficient Back-Reflective Scattering Contact-Electrode for Thin-Film Solar Cells

Xuejiao Liang, [†a] Bofei Liu, [†a] Lisha Bai, [a] Junhui Liang, [a] Haibo Gao, [a] Ying Zhao, [a] and Xiaodan Zhang* [a]

Institute of Photo Electronics Thin Film Devices and Technology of Nankai University, Key Laboratory of Photoelectronic Thin Film Devices and Technology, Tianjin 300071, P. R. China

Abstract

The integration of periodic back reflectors in thin-film solar cells offers the potential to accurately control the scattering behavior and improve the absorption enhancement in active layers, thereby overcoming the inherent performance limitations imposed by their poor light absorption and carrier collection. Periodically textured metal electrodes were therefore fabricated using a unique sauna-like method, and were investigated both experimentally and theoretically. In this way, we confirm the effectiveness of tuning the geometric parameters and corresponding surface morphology on enhancing the diffraction behavior and light absorption through rigorous coupled wave analysis (RCWA) and finite-difference time-domain (FDTD) simulation. Furthermore, the periodically textured metal electrodes produced by this unique fabrication process provide a means of enhancing absorption in the long wavelength range, thus opening a new way to further improve the performance of thin-film solar cells.

Keywords: Periodically textured metal electrode; sauna-like method; finite difference time domain (FDTD) analysis; hydrogenated microcrystalline silicon

Introduction

A number of critical advantages have been found in the use of thin film photovoltaic solar cells in place of traditional crystalline-silicon solar cells, which

include a lower cost and reduced material usage. Nevertheless, these advantages typically come at the expense of reduced efficiency owing to the restrictions placed on the thickness of the active layer by the high defect density, Urbach energy, and reduced carrier diffusion length of amorphous, microcrystalline, and polycrystalline silicon.[1-3] Although the poor light absorption in the intrinsic layer imposes a limit on the extent to which the efficiency of thin-film solar cells can be improved, this bottleneck can conceivably be overcome by incorporating thicker intrinsic layers of least ten micrometers to ensure that all of the photons are absorbed.[4] However, the greatly increased electrical loss that results from a lower carrier collection makes such an option impractical. Consequently, there is high demand to find a more suitable means to improve the optical absorption, carrier excitation, and photocurrent generation in the active layer of thin-film solar cells, without suppressing the electrical collection of the generated carriers.

With this in mind, a number of light-trapping methods have been proposed in recent years that have been aimed at elevating the light coupling, trapping, and resulting light absorption of intrinsic layers, e.g., in photonic crystals,[5-7] nanowires, [8,9] gratings, [6,10,11] plasmonic nanostructures, [12,13] anti-reflection coatings [14] and Mie resonators[15]. These light trapping schemes have been successfully proven in increasing the light absorption in intrinsic layers, as well as improving the photocurrent output. Not only that, but the rough interfaces produced at the front or back of the active material can also increase the optical path length of the light by scattering, which consequently enhances its absorption.[16-18] It should be noted, however, that attention has tended to focus on enhancing the absorption of long-wavelength light, which intrinsically has a low absorption coefficient and is difficult to be trapped. A conventional solution to this lies in the use of a metal-back reflective contact such as Ag or ZnO/Ag, which can provide excellent conductivity and good reflectivity. As such, thermally roughened silver films, silver-covered randomly oriented SnO_2 and ZnO pyramids grown by chemical vapor deposition and silver-covered vertically aligned ZnO nanorods grown by hydrothermal synthesis

have already been successfully used to enhance the infrared light absorption of n-i-p type solar cells.[19, 20]

With the exception of optimizing conventional textured back reflectors to the absorption of infrared light,[21] the focus in recent years has been on the use of periodically textured substrates or surface gratings as a more sophisticated platform to achieve higher current densities. Unlike the continuous scattering of incoming broadband light across a wide range of angles[22] that occurs with textured surfaces, periodic surface gratings allow for the incoming light to be selectively diffracted along certain angles (angle-selective scattering)[23] by controlling the surface geometry. Owing to the simplicity and uniformity of their textured morphology, periodic structures also have the potential to provide a much clearer correlation between texture and the photovoltaic performance of solar cells.[24] However, the experimental fabrication of periodically textured substrates on a larger scale, with fewer defects in two-dimensional space, and with precise control over surface morphology parameters such as height, period, duty cycle and geometry is still the subject of research.

There are several papers reporting the use of periodic electrodes to enhance light trapping[12,19,25-27]. Such as, large-scale quasi-ordered nanodent arrays are acquired on Al foils by electrochemically anodizing; conformal Ag films are used as the back reflectors by direct current sputtering in hydrogenated amorphous silicon (a-Si:H) solar cells; [12] Reactive ion etching (RIE), in which SiO_2 nanospheres are used as a mask to fabricate a periodic nanostructure; [19,27] The other viable alternatives, for example, photolithography[24], which adopts a photoresist in combination with surface etching and successfully be applied in thin-film hydrogenated microcrystalline silicon (μc-Si:H) solar cells, can provide an alternative in some instances, however, is limited by its complexity.

Despite the aforementioned fabrication methods, in this paper, we propose a new "sauna-like" method for producing large areas of periodically textured metal electrodes for the first time. The performance of these electrodes is evaluated both

experimentally and theoretically, with a view to their potential to enhance the absorption of incoming light and short-circuit current density in μc-Si: H thin-film solar cells.

Experimental

The first, and arguably most critical, stage in the fabrication of the periodically textured metal electrodes in this study was hexagonal monolayer and closely arranged polystyrene (PS) microspheres that served as a mask. Due to this reason, the glass substrate for the electrodes was first thoroughly cleaned for more than 5 hours in a H_2SO_4/H_2O_2 (2:1) piranha solution, and then rinsed for 10 min in deionized water. Next, an emulsion solution of PS microspheres was dropped vertically onto the cleaned glass, and then dried at room temperature. At this point, the PS microspheres were heterogeneously distributed as multiple layers over the surface of the glass. Once the sample was completely dry, steam was applied to cause the PS microspheres to shrink and self-assemble, this process defining the sauna-like method. This application of steam was subsequently found to produce hexagonally monolayer and closely arranged PS microspheres. A schematic diagram of this sauna-like method is shown in Fig.1, in which the two inset pictures show the appearance of the PS microspheres before and after self-assembly.

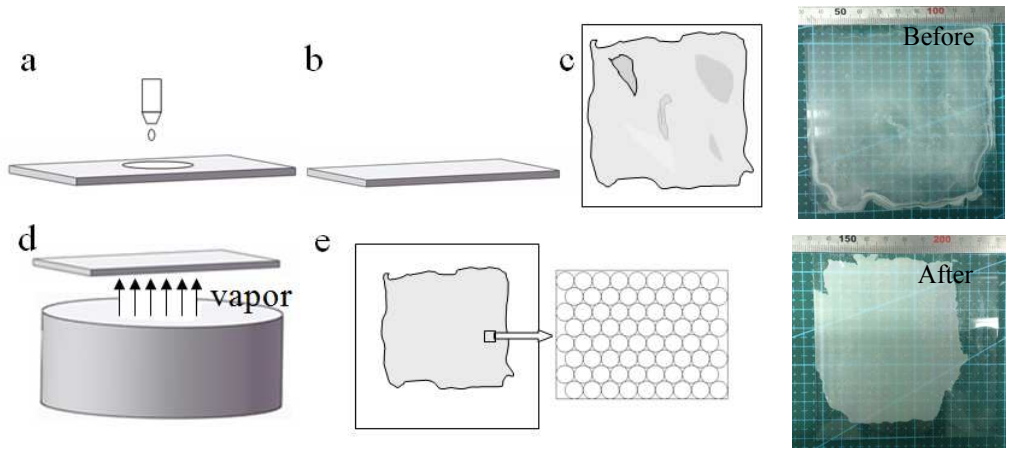

Fig.1 Schematic diagram of the sauna-like method. a) Drop the PS microspheres emulsion solution vertically to a glass substrate. b) Drying at room temperature. c) Heterogeneous and multilayered structure. d) Steam is applied to re-assemble the heterogeneous PS microspheres. e) Hexagonally monolayer and closely arranged PS microspheres. The two inset pictures show the

material before and after the sauna-like process (d).

Fig.2 illustrates the major steps involved in the fabrication of the periodically textured metal electrodes. In this, reactive ion etching (RIE) with O_2 gas was used to first shrink the PS microspheres. An initial Ag film was then deposited by magnetron sputtering, after which the PS microspheres were removed ultrasonically to leave a substrate with a periodic structure. Finally, a second layer of Ag film was deposited on the substrate to fill the vacancies left under the PS microspheres.

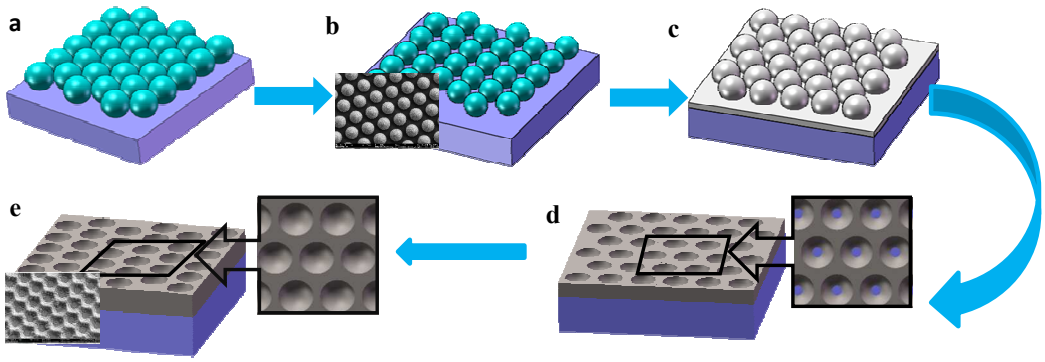

Fig.2. Schematic diagram depicting the fabrication of periodically textured metal electrodes: a) hexagonally monolayer and closely arranged PS microspheres; b) PS microspheres after RIE; c) Deposition of an Ag film; d) Ultrasonic removal of PS microspheres from the substrate; e) Deposition of a second Ag film on the substrate.

Optical performance simulations were accomplished by employing rigorous coupled wave analysis (RCWA) of the device structure shown in Fig.2d. The μc-Si:H solar cell structures deposited on this periodically textured metal electrode were also simulated by a finite-difference time-domain (FDTD) method to determine the light response in the corresponding intrinsic layers. To compare the effect of the periodically textured metal electrode's geometry on the optical properties, it was important to ascertain the precise shape of the fabricated cells. Consequently, we imported the cross-sectional profiles obtained experimentally by atomic force microscope (AFM) scans into the RCWA and FDTD models to more accurately reflect the true structure. Similarly, the experimentally determined optical constants for each layer of the structure were also taken into account.

Both SUPRA 55VP scanning electronic microscopy (SEM) (Carl ZEISS AG, Jena, Germany) and SPA 400 AFM (SII Nanotechnology, Inc., Tokyo, Japan) were employed to characterize the surface morphology. The optical reflection spectra were measured within the spectrum range of 300 to 1100 nm using a Cary 5000 spectrophotometer (Varian Co., Palo Alto, USA) equipped with an integrated sphere.

Results and Discussion

The influence of the variation of the etching time on the size of the PS microspheres is illustrated in Fig.3a. We can see that with an increase in the etching time the diameter of the PS microsphere becomes smaller. This is confirmed by the SEM images of PS microspheres etched for 8 and 10 min that are given in Fig.3b. These figures demonstrate that with a reduction in the diameter of the PS microspheres, the height of the periodically textured Ag electrode increases. Furthermore, the decrease in the distance between the periodically arranged PS microspheres as their diameter is increased makes it increasingly difficult for the sputtered silver atoms to infiltrate the spaces between them. The cross-sectional profiles obtained from the AFM scans in Fig.3c1-f1 were statistically summarized into five key parameters, as presented in Fig.3g.

As shown in Table 1, a reduction in the diameter of the PS microspheres from 1.8 to 1.4 μm causes an increase in the W_{bottom}, H, α, and β values of the electrode. Moreover, Fig.4a demonstrates that there is a change in the total and diffuse reflectivity spectra that is coincident with this change in morphology. Thus, a remarkable increase in the diffuse reflection was found to accompany the reduction in the diameter of the PS microspheres to 1.4 μm.

a

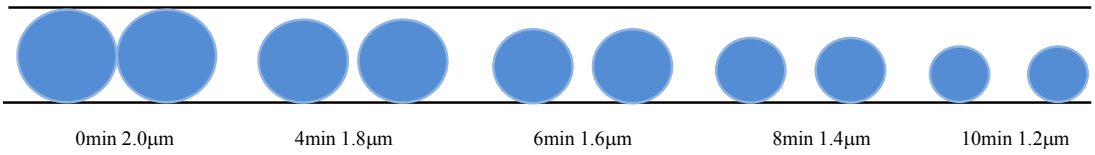

b

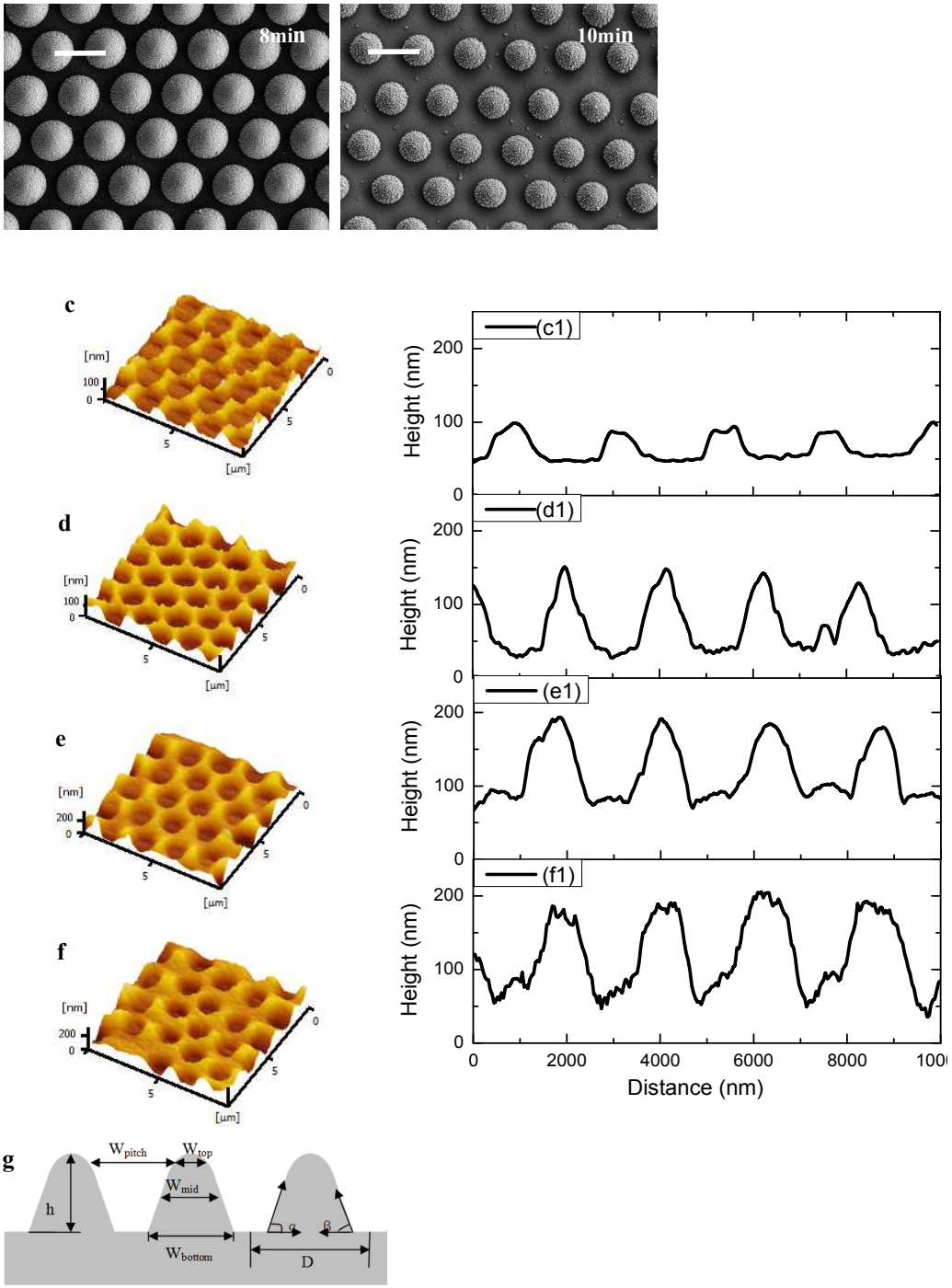

Fig.3 a) Schematic diagram of PS microspheres with different etching times. b) SEM images of PS microspheres after 8 and 10 min of etching. c-f) AFM images of periodically textured Ag electrodes with etching times of: 4, 6, 8, and 10 min. The deposition time of silver is identical in all instances and the cross-sectional profiles are given in c1-f1. g) Schematic diagram depicting the cross-sectional profile of a periodically textured Ag electrode based on the AFM images.

Table 1 The distance (*D*) between PS microspheres, angular parameters, α and β, height (H) and width (W_{bottom}), of the electrode cone, and RMS of fabricated samples.

Diameter of the etched balls [μm]	H [nm]	$W_{bottom.}$ [nm]	α [°]	β [°]	RMS [nm]
1.8 μm	50	1092	5.7	5.6	18
1.6 μm	108	1174	10.8	10.2	38
1.4 μm	130	1358	11.7	14.6	48
1.2 μm	148	1512	12.7	10.4	48

The influence of an electrode's surface morphology on wave propagation can be more thoroughly understood by determining the diffraction efficiency of the reflected waves as a function of their diffraction order and incident wavelength. In this study, the diffraction behavior was analyzed by RCWA,[28, 29] which provides a distinct measure of the reflected light distribution and comparative evaluation of the distance between PS microspheres. The diffraction patterns for electrodes with 1.8 and 1.2 μm PS microspheres, as shown in Fig.4b and 4c, were calculated based on the structure depicted in Fig.4d. The experimentally determined cross-sectional profiles of the two samples (Fig.3) were taken into account, along with the experimentally measured thickness of the various layers of the Air/Glass/Ag/ZnO/Air structure. The simulated results for the total and diffuse reflection of the two substrates are shown in Fig.4e, with the total reflection of almost 100 % and overall trend being virtually the same as that for the experimental observations.

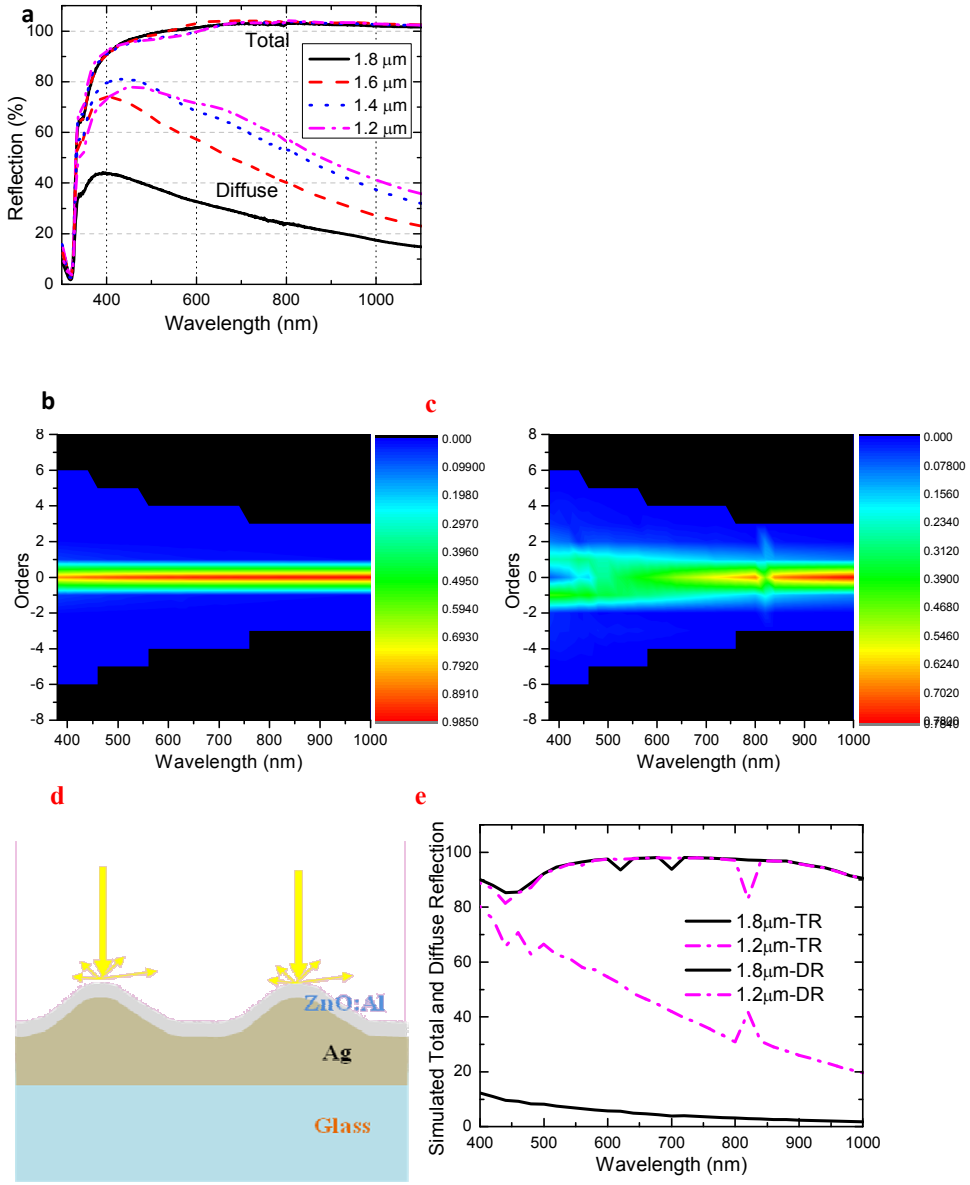

Fig.4 a) Total and diffuse reflection spectra of periodically textured metal electrodes with the same deposition time. The diameters of the PS microspheres are 1.8, 1.6, 1.4, and 1.2 μm. b) The diffraction pattern of the sample 1.8 μm PS microspheres. c) The diffraction pattern of the sample 1.2 μm PS microspheres. d) The schematic structure of the periodically textured metal electrodes. e) The simulated total reflection and diffuse reflection of the two substrates

As illustrated in Fig.4b, the electrode of 1.8 μm PS microspheres diffracts more 0^{th} order waves, thus increasing its specular reflection. Conversely, when the size of PS microspheres decreases to 1.2 μm, most of the light energy is coupled to

diffraction orders other than the 0^{th} order, thus increasing the diffused reflection. This results in the very obvious difference in the contribution of diffusion to the total reflection indicated in Fig.4e. Furthermore, this means that the distribution of reflected energy is directly related to the surface morphology on which the incoming light shines, i.e., the height (H) and width (W_{bottom}) of the diffraction unit; the greater height (148 nm, in Table 1) of the 1.2 μm PS microspheres than that of the 1.8 μm PS microspheres (50 nm) gave rise to the variation in energy distribution. This variation in phase in relation to height can be calculated by the following formula: [30]

$$\phi_d = \frac{4\pi}{\lambda} n_{air} h \quad (1)$$

where n_{air} is the refractive index of air, h is the height of the diffraction unit and λ is the wavelength of the incoming light. Since the refractive index of the incident medium (air) is 1.0, the phase difference is only related to the height of the diffraction unit and the wavelength of the incoming light. A phase change of $(2n-1)\pi$ (n = 1,3,5,...) will therefore result in the propagation of odd diffraction orders[31], whereas $2n\pi$(n = 0,2,4,…) corresponds to odd diffraction orders. Based on the concept, we can estimate the maximum possible phase change for the two samples based on a smallest wavelength of 400 nm and a peak-to-peak value of 50 and 148 nm. The resulting values of $\varphi_{1.8} < 0.5\pi$ and $\varphi_{1.2} < 1.48\pi$ confirm that more light is concentrated in the 0^{th} order when the electrode is periodically textured with 1.8 μm PS microspheres. Meanwhile, the formula also illustrates that the reduction in phase difference with wavelength will lead to a greater specular component at longer wavelengths, as is shown in Fig.4b and 4c.

We can also see that an increase in wavelength should result in less diffraction orders; the diffraction order, m, and the diffraction angle, θ_m, can be expressed as a function of the diffraction unit's period, P [30]:

$$Pn\sin(\theta_m) = m\lambda \quad (2)$$

The diffraction order (m) should be less than Pn/λ($m \leq Pn/\lambda$), with a smaller period or longer wavelength reducing the number of orders of diffraction. This explains the

black zones where no reflected light occurred in Fig.4b,c. However, even with the 1.2 μm PS microspheres producing a larger period of 1512 nm (Table 1), the change in W_{bottom} from 1092 to 1512 nm is only sufficient to change the diffraction angle, not the diffraction order.

From the results presented thus far, it is evident that adjusting the etching time to fine-tune the diameter of the PS microspheres can be used to control the surface morphology and scattering properties of periodically textured Ag electrodes. However, as Fig. 4a illustrates, the diffuse reflection at longer wavelengths still shows a low scattering of light. Consequently, in order to further improve the light scattering properties, we shifted our focus to thickness of the first layer of Ag film. Therefore, nominal thicknesses of 149, 356 and 430 nm were evaluated, with the nominal thickness of the second layer remaining constant at 340 nm.

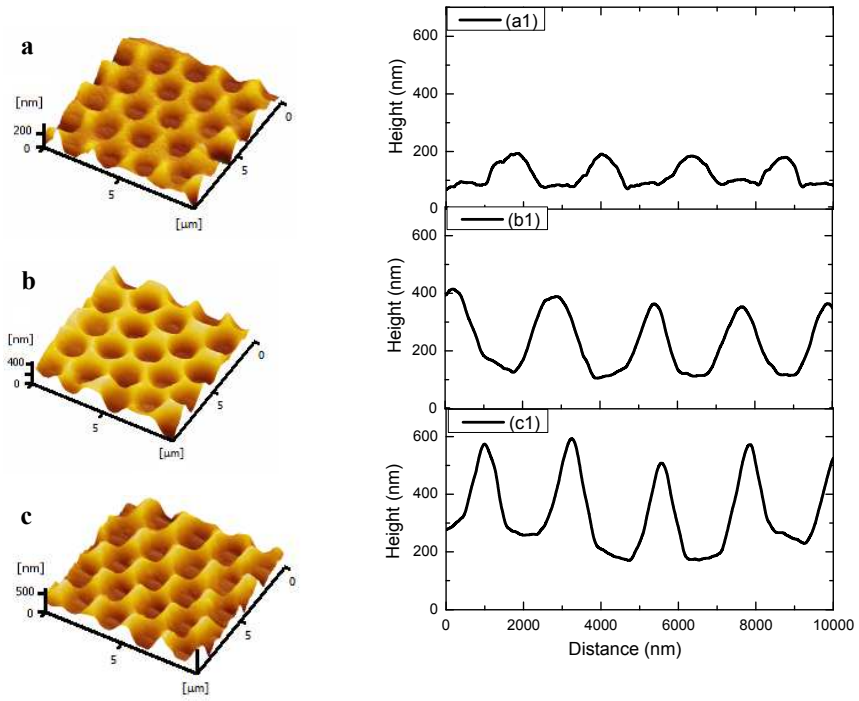

Fig.5 a-c) AFM images of periodically textured micro-scale back reflectors with nominal first-layer thicknesses of 149, 356, and 430 nm. The cross-sectional profiles of these electrodes are given in a1-c1. The nominal thickness of the second layer is 340 nm.

Fig.5 shows AFM images and cross-sectional profiles of the periodically textured Ag electrodes produced with nominal first-layer thicknesses of 149, 356 and 430 nm,

with their related statistical parameters summarized in Table 2. From this, we can see that with an increase in the nominal thickness of the first layer, the height of the electrode increases from 130 to 409 nm. This, in turn, increases the W_{bottom}, H, RMS, α and β values of the periodically textured Ag electrode. However, when compared to the effect of varying the etching time, this modification of the nominal thickness of the first layers clearly has a far more significant impact on the electrode height.

Table 2 The distance (D) between PS microspheres, angular parameters, α and β, height (H) and width (W_{bottom}) of the electrode cone, and RMS of fabricated samples

Diameter of the etched balls [μm]	Silver thickness [nm]	H [nm]	W_{bottom} [nm]	α [°]	β [°]	RMS [nm]
1.4	149	130	1358	11.7	14.6	48nm
1.4	356	255	1486	18.6	21.8	93nm
1.4	430	409	1551	31.2	27.4	138nm

Fig.6a depicts the total and diffuse reflectivity spectra of the periodically textured Ag electrodes, which correspond with their difference in morphology. For instance, with an increase in the nominal thickness from 149 to 356 nm, a remarkable increase of 20 % in diffuse reflection is observed at longer wavelengths (800 nm). The RCWA-simulated total and diffuse reflectivity spectra exhibit a similar trend to the measured spectra, as shown in Fig.6b. Fig.6c shows the normalized and time-averaged E-field distribution for a periodically textured Ag electrode with a nominal thickness of 430 nm under illumination at a wavelength of 900 nm. In this, any incoming photons reaching the ZnO/Ag interface are reflected back into the surrounding medium (air), following partial absorption in the Al doped zinc oxide (ZnO:Al)medium. The constructive and destructive interference that occurs between the incoming and reflected light results in a diffraction distribution containing both hot and cool spots. Unlike the layered distribution of the E-field observed in the periodically textured Ag electrode with a nominal thickness of 149nm, this non-layered distribution of the E-field created by a 430 nm thick film is indicative of more light being diffracted in a non-zero order.

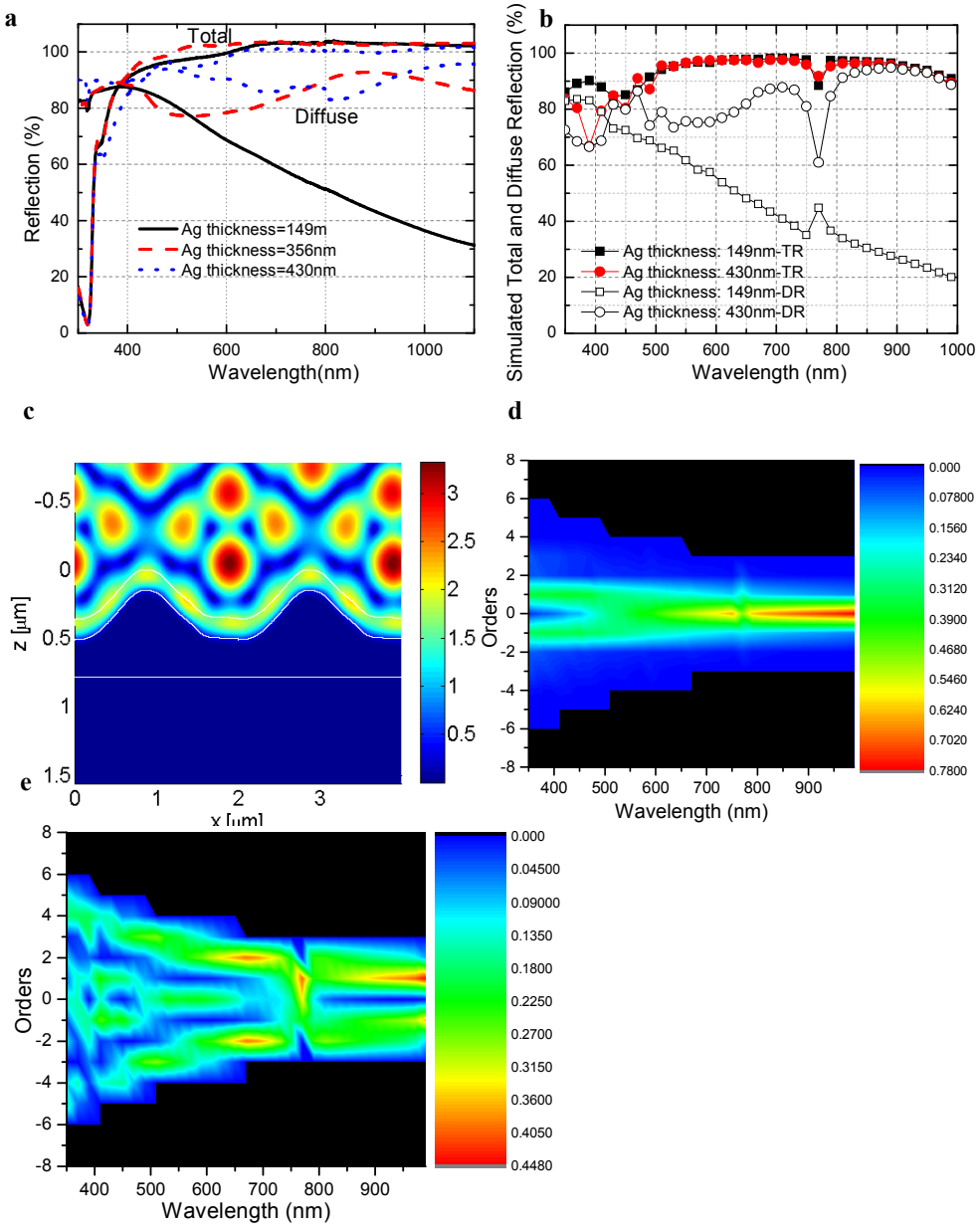

Fig.6 a) Measured total reflection and diffuse reflection corresponding to Ag thicknesses of 149, 356, and 430 nm. b) Total reflection and diffuse reflection from RCWA simulation for Ag thicknesses of 149 and 430 nm. c) Normalized and time-averaged E-field distribution in a periodically textured Ag electrode with a nominal thickness of 430 nm under illumination at a wavelength of 900 nm. The diffraction pattern in reflection for Ag thicknesses of d) 149 nm and e) 430 nm.

The diffraction patterns of samples with nominal first-layer thicknesses of 149 and 430 nm are shown in Fig.6d and 6e, in which the hot spots of the 149 nm sample at wavelengths of 700 to 1000 nm indicate a high specular reflection. In contrast, such hot spots at long wavelengths are only evident in the 430 nm thick sample at non-zero diffraction orders, specifically $\pm 1^{st}$ and $\pm 2^{nd}$ orders. Moreover, more light energy is

coupled in these higher orders when compared to the 149 nm sample. This of course can be attributed to the obvious difference in height between the 130 and 409 nm textured electrodes.

However, the effect of increasing the electrode height does have its limitations, as greater thicknesses were found to make it impossible to ultrasonically remove the PS microspheres. Nevertheless, increasing the nominal thicknesses of the first Ag layer is more effective at enhancing the scattering of long wavelength light than varying the PS microsphere etching time. This is particular significance to the infrared response of microcrystalline silicon (μc-Si:H) solar cells with the improved wide spectra absorption, which have an inherently low absorption at long wavelengths.

To evaluate the effect of periodic substrates on the light absorption of solar cells, simulative external quantum efficiency (EQE) spectra of n-i-p μc-Si:H solar cells with an Ag thickness of 149 and 430 nm were obtained by FDTD[32], and are shown in Fig.7a. These calculations were based on the solar cell structure (Air/Glass/Ag/ZnO:Al/P (20 nm)/μc-Si:H (1500 nm)/N (30 nm)/ITO (90 nm)/Air) depicted in Fig.7b. To better illustrate the effect of surface profile on light absorption, the profiles obtained by AFM scans were used in a 2-D FDTD calculation. Similarly, the thickness of all the layers was measured by individual material experiments and the complex optical constants were determined by measurements with proper medium dispersion formulas.[33,34] Considering the reason that the hexagonally arranged structure is polarization independent[12,35], the polarization of the incoming light was assumed to be transverse electric (TE), whilst the thickness of the intrinsic layer (μc-Si:H) was defined as 1500 nm. The absorption in the intrinsic layer can therefore be calculated from the divergence of the Poynting vector: [36]

$$Q_{abs} = \frac{1}{2}\left(\omega\varepsilon'' \left|\mathrm{E}\right|^2 + \omega\mu'' \left|\mathrm{H}\right|^2\right) \quad (3)$$

where E and H are the electric and magnetic fields in the μc-Si:H layer, respectively, and are calculated by FDTD; ω is the frequency; and ε" and μ" are the respective imaginary parts of the permittivity and permeability. When using μc-Si:H, μ" = 0 and the external quantum efficiency EQE in the μc-Si:H layer can be calculated as:[32]

$$EQE = \frac{1}{P_{inp}} \int \frac{1}{2} c\varepsilon_0 n\alpha \left|\mathrm{E}(x, z)\right|^2 dxdz \quad (4)$$

where P_{inp} is the total power incident on the periodic unit cell (= 1 W in this study), c

is the speed of light in a vacuum, ε_0 the free space permittivity, n is the refractive index at a given point (x,z) and α is the absorption coefficient.

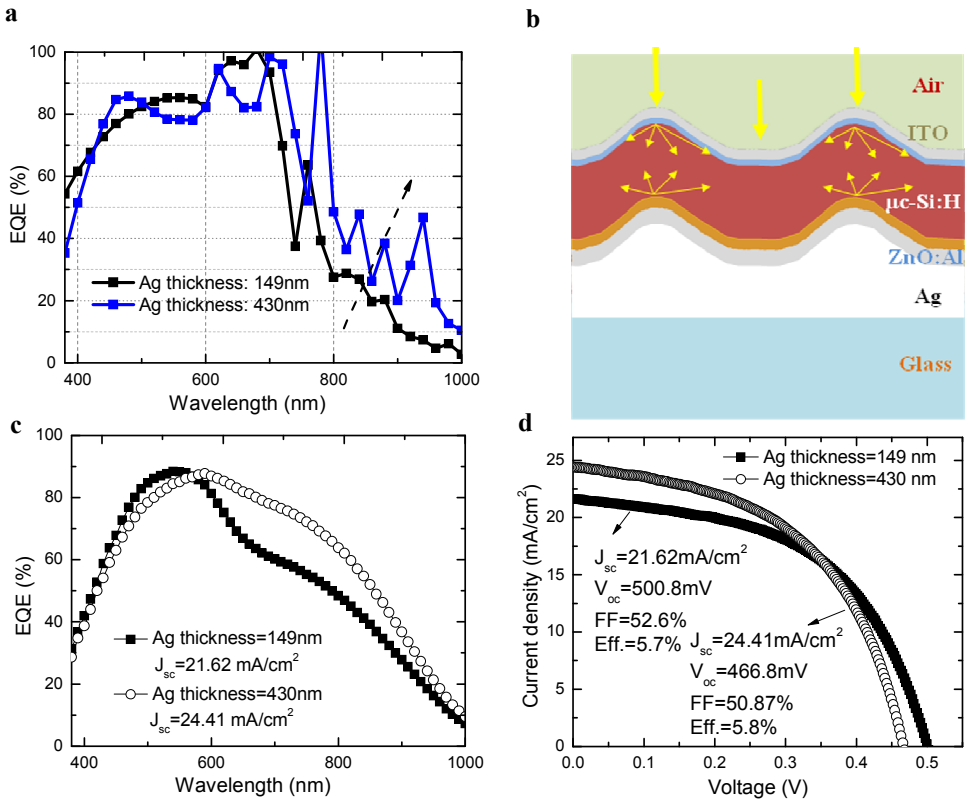

Fig.7 a) Simulated EQE spectra of n-i-p μc-Si: H solar cells with Ag back reflectors of various thicknesses. b) Schematic of the n-i-p device structure simulated by FDTD. c) Measured EQE and d) J-V curves of the fabricated n-i-p μc-Si: H solar cells.

Fig.7a and 7c show the simulated and measured EQE curves for solar cells deposited on periodically textured Ag electrodes with a nominal thickness of 149 and 430 nm, respectively. From these curves, we can see that the response in the wavelength range of 700–1000 nm is enhanced by an increase in Ag thickness. This enhancement is also found in the measured EQE curves, and there is a consistent trend between the simulated and measured results, confirms that it is the result of the enhanced light diffusion and confinement demonstrated in Fig. 6a, b.

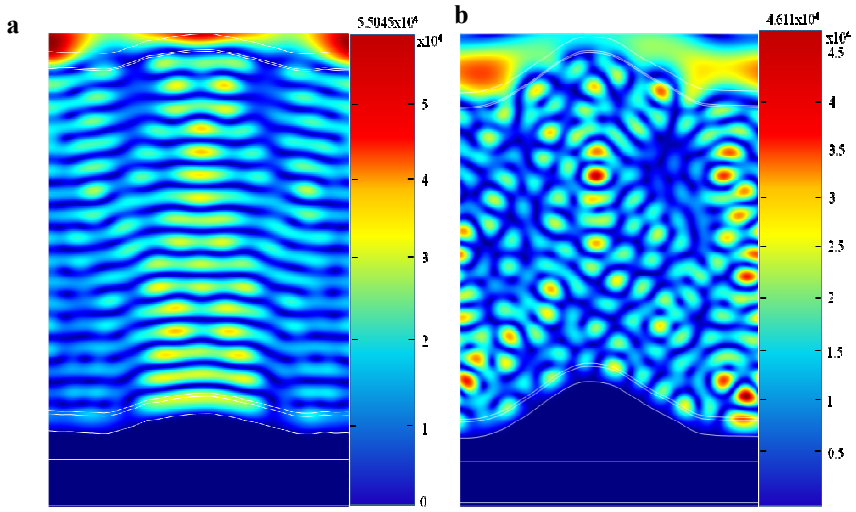

Fig.8 Time-averaged E-field distribution of μc-Si:H solar cells deposited on periodically textured Ag electrodes with a nominal thickness of a) 149nm and b) 430nm under illumination at a wavelength of 900nm.

To provide a deeper insight into the change in wave propagation and absorption resulting from modification of the surface morphology, time-averaged E-field distributions of cells fabricated on periodically textured Ag electrodes with nominal thicknesses of 149 and 430nm under illumination at a wavelength of 900 nm are presented in Fig.8. This shows that owing to the low absorption coefficient of μc-Si:H materials at long wavelengths, the incident light makes multiple passes through absorber and so a high E-field intensity is still present in the vicinity of the μc-Si:H/ZnO interface in Fig.8a and 8b. Moreover, a large difference between the E-field distributions of the two samples is clearly evident, which may be related to the different surface profiles and their associated phase differences. The layered interference pattern, with its well-defined destructive and constructive regions, originates from the high specular diffraction and interference of 0^{th} order incoming and reflected waves, as shown in Fig.6a and 6d. In the case of the 149 nm μc-Si:H cell the strongest E-field intensity predominantly occurs in the regions of greatest height, which can simply be attributed to a lightning rod effect.[37] However, with the 430 nm μc-Si:H cell, an interference pattern with distributed destructive and constructive regions is indicative of higher diffusion resulting from the higher peak height, as shown in Fig.6a and 6e. This can be explained by incoming waves being diffracted by

the front interface and interfering with reflected waves of different orders, as well as non-zero order waves from adjacent periodic units, giving rise to a distribution of destructive and constructive regions. Hot spots resulting from constructive interference contribute mainly to the power absorption, and thus the variation in E-field distribution results in the enhanced long-wavelength light trapping of the 430 nm μc-Si:H cell, as presented in Fig.7c. The strongest absorption in Ag metal is within a skin depth of the first few nanometers. [36]

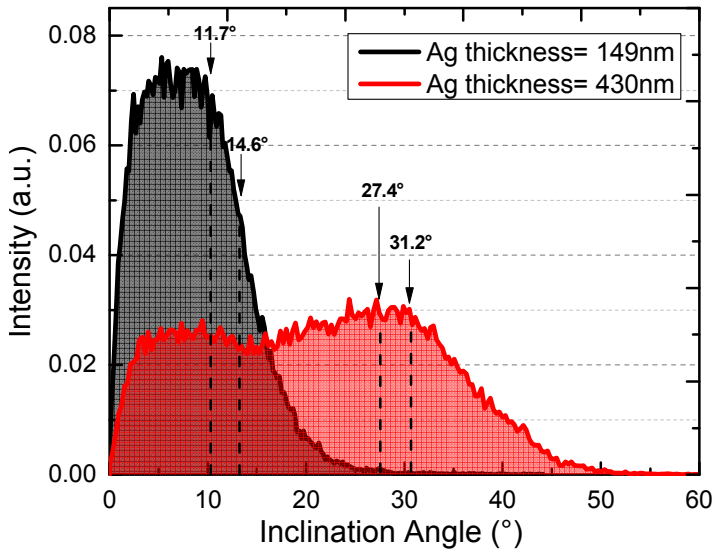

Fig.9 Inclination angle distribution of periodically textured Ag electrodes with a nominal thickness of 149 and 430 nm. The angle parameters, α and β, are also depicted.

With the obvious exception of the enhanced long wavelength absorption observed with a greater nominal thickness of Ag layer, it is well known that textured substrates typically deteriorate the open-circuit voltage V_{oc} and fill factor *FF* of thin-film silicon solar cells.[38] As shown in Fig.7d, the detrimental effect of about 34 mV of V_{oc} loss and apparent reduction in *FF* from 52.6 to 50.87 % exceeds the gain achieved in J_{sc}. This electrical reduction may originate from texture-induced cracks that penetrate the μc-Si:H intrinsic layer along the growth direction, which give rise to a greater density of defects and voids in the absorber that can directly influence the electrical performance of the deposited solar cells. Given this reason, the inclination angle distributions of the surface morphologies of the samples, as calculated from the

corresponding AFM scans, are presented in Fig.9. The angular parameters, α and β, are also noted on these curves. As can be seen, the broader angle distribution of 20° to 50° for the 430 nm periodically textured Ag electrode is comparable to the inclination angle of about 45° of low pressure chemical vapor deposition (LPCVD) deposited on a ZnO:B substrate, in which a large electrical reduction due to texture-induced cracks is always observed.[39] This proves that the reduction of V_{oc} and *FF* evident in Fig.7a is the result of cracks induced by periodic units with a large inclination angle. We can also see that the values of α and β are also approximately equal in the angular region with high intensity. This means that the electrical loss of cells deposited on periodically textured Ag electrodes can be easily characterized by just two geometric parameters. For example, if α and β are larger than 20° then this is likely to lead to a loss of V_{oc} and *FF*. By tuning α and β to ensure that they are less than 20°, the adverse effects of electrical can be mitigated, thereby enhancing any related improvement in cell efficiency.

However, it should be noted that a much low resistance for solar cells deposited on periodically textured Ag electrodes with a nominal thickness of 149 and 430 nm was found in Fig.7d, which is the reason why the FF of the cells was still 52.6% in spite of utilizing the substrates with inclination angles below 20°. This large shunting phenomenon, which origined from our bad design of Al front metal electrodes at that time, were fully realized and mitigated with newly designed Al front metal electrodes . Finally, with the further optimization of the fabrication process and device design of μc-Si: H solar cells, and the application of newly designed front metal electrodes, the EQE and J-V characteristics of the optimized μc-Si: H solar cells produced in this study are summarized in Fig.10. The high efficiency of 8.56 %, J_{sc} of 24.05 mA/cm^2, V_{oc} of 498.6 mV and *FF* of 70.57 % all indicate that periodically textured metal electrodes offer many advantages for use in μc-Si:H cells.

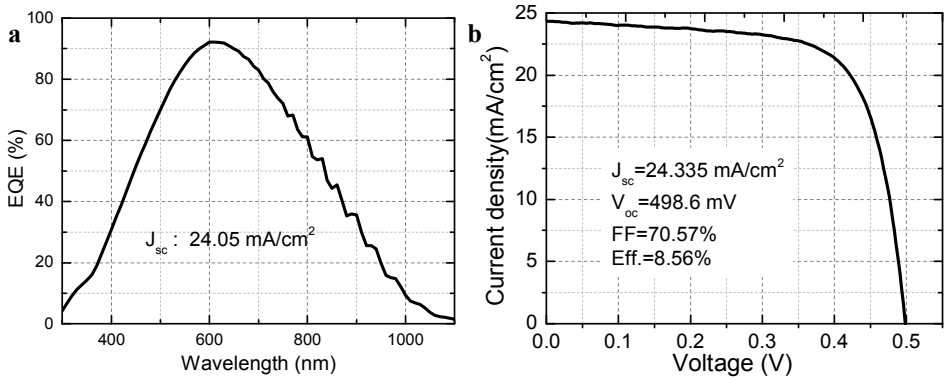

Fig.10 a) External quantum efficiency and b) J-V curve under AM 1.5 irradiation of n-i-p μc-Si: H solar cells fabricated on optimized periodically textured metal electrodes

Conclusions

A unique "sauna-like" method is proposed for the fabrication of periodically textured metal electrodes, using which geometrical parameters such as height, duty cycle, period, and inclination angle can all be accurately controlled by adjusting the etching times of the PS microspheres and the nominal thickness of the Ag film used. This level of control was found to be effective in altering the diffraction behavior of reflected waves by varying the surface morphology. The agreement between observations of experimental fabrication and theoretical calculation proves the feasibility of this type of periodic substrate in improving the long-wavelength absorption of microcrystalline silicon solar cells. Furthermore, this fabrication process can be expanded beyond n-i-p type μc-Si:H single-junction solar cells, with the potential for application to the transparent conductive oxide films of p-i-n type silicon-based solar cells, or even cells utilizing organic, CdTe, or crystalline silicon active materials.

Acknowledgments

We are grateful for financial support from the National Basic Research Program of China (Grant Nos. 2011CBA00706, No.2011CBA00707), Science and Technology Support Program in Tianjin (12ZCZDGX03600), Major Science and Technology Support Project of Tianjin City (No. 11TXSYGX22100), and Specialized Research Fund for the PhD Program of Higher Education (20120031110039).

Notes

[a] *Institute of Photo Electronics Thin Film Devices and Technology of Nankai University, Key Laboratory of Photo Electronics Thin Film Devices and Technology of Tianjin, Key Laboratory of Opto Electronic Information Science and Technology, Ministry of Education, Tianjin, 300071, PR China. Fax: +86 22-23499304; Tel: +86-22-23499304 E-mail: xdzhang@nankai.edu.cn*

† These authors contributed equally to the work.

* Corresponding Authors, E-mail: xdzhang@nankai.edu.cn

Author Contributions

Xuejiao Liang prepared and characterized the substrates and also wrote the manuscript, Bofei Liu simulated and wrote the manuscript, Lisha Bai prepared the solar cells, Junhui Liang fabricated ZnO films, Haibo Gao proposed Sauna-Like method. Ying Zhao initiated the research, Xiaodan Zhang initiated the research, designed the devices, supervised the work and revise the manuscript. The authors declare no competing financial interest.

References

[1] G.D. Cody, T. Tiedje, B. Abeles, B. Brooks, Y. Goldstein, *Phys. Rev. Lett.*, 1981, **47**, 1480.

[2] A. Matsuda, *J. Non-Cryst. Solids,* 2004, **338**, 1.

[3] J. K. Rath, *Sol. Energy Mater. Sol. Cells,* 2003, **76**, 431.

[4] W. Wang, S. Wu, K. Reinhardt, Y. Lu, S. Chen, *Nano Lett.,* 2010, **10**, 2012.

[5] S. B. Mallick, M. Agrawal, P. Peumans, *Opt. Express,* 2010, **18** , 5691.

[6] J. Üpping, A. Bielawny, R. B. Wehrspohn, T. Beckers, R. Carius, U. Rau, R. Zentel, *Advanced Materials,* 2011, **23**, 3896.

[7] P. Bermel, C. Luo, L. Zeng, L. C. Kimerling, J. D. Joannopoulos, *Opt. Express,* 2007, **15**, 16986.

[8] M. J. Naughton, K. Kempa, Z. F. Ren, Y. Gao, J. Rybczynski, N. Argenti, W. Gao, Y. Wang, Y. Peng, J. R. Naughton, *Phys. Status Solidi RRL,* 2010, **4**, 181.

[9] E. Garnett, P. Yang, *Nano Lett.,* 2010, **10**, 1082.

[10] S. I. Na, S. S. Kim, J. Jo, S. H. Oh, J. Kim, D. Y. Kim, *Adv. Funct. Mater.,* 2008, **18**, 3956.

[11] C. Battaglia, J. Escarré, K. Söderström, M. Charrière, M. Despeisse, F. J. Haug, C. Ballif, *Nature Photonics,* 2011, **5**, 535.

[12] H. Huang, L. Lu, J. Wang, J. Yang, S. F. Leung, Y. Wang, Z. Fan, *Energy Environ. Sci.,* 2013, **6**, 2965.

[13] N. N. Lal, B. F. Soares, J. K. Sinha, F. Huang, S. Mahajan, P. N. Bartlett, N. C. Greenham, J. J. Baumberg, *Opt. Express,* 2011, **19**, 11256.

[14] L. Schirone, G. Sotgiu, F. P. Califano, *Thin Solid Films,* 1997, **297**, 296.

[15] S. A. Mann, R. R. Grote, R. M. Osgood, J. A. Schuller, *Opt. Express,* 2011, **19**, 25729.

[16] J. Müller, B. Rech, J. Springer, M. Vanecek, *Sol. Energy,* 2004, **77**, 917.

[17] A. Poruba, A. Fejfar, Z. Remeš, J. Špringer, M. Vaněček, J. Kočka, J. Meier, P. Torres, A. Shah, *J. Appl. Phys.,* 2000, **88**, 148.

[18] R. H. Franken, R. L. Stolk, H. Li, C. H. M. van der Werf, J. K. Rath, R. E. I. Schropp, *J. Appl. Phys.,* 2007, **102**, 014503.

[19] C. M. Hsu, C. Battaglia, C. Pahud, Z. Ruan, F. J. Haug, S. Fan, Y. Cui, *Adv. Energy Mater.,* 2012, **2**, 628.

[20] T. Söderström, F.-J. Huag, V. Terrazzoni-Daudrix, C. Ballif, *J. Appl. Phys.,* 2008, **103**, 114509.

[21] A. M. K. Dagamseh, B. Vet, F. D. Tichelaar, P. Sutta, M. Zeman, *Thin Solid Films,* 2008, **516**, 7844.

[22] C. Battaglia, C. M. Hsu, K. Söderström, J. Escarré, F-J. Haug, M. Charrière, M. Boccard, M. Despeisse, D. T. L. Alexander, M. Cantoni, Y. Cui, C. Ballif, *ACS nano*, 2012, **6**, 2790.

[23] O. Isabella, A. Campa, M. C. R. Heijna, W. Soppe, R. van Erven, R. H. Franken, H. Borg, M. Zeman, *Conference Record of the 23rd European Photovoltaic Solar Energy Conference,* 2008, 2320.

[24] H. Sai, K. Saito, N. Hozuki, M. Kondo, *J. Appl. Phys.,* 2013, **102**, 053509.

[25]HL Chen, SY Chuang, CH Lin, YH Lin, *Opt. Express*, 2007, **15**,14793.

[26] WC Tu, YT Chang, CH Yang, DJ Yeh, CI Ho, CY Hsueh, SC Lee, *Appl. Phys. Lett.,* 2010, **97**,193109.

[27] J. Zhu, C. M. Hsu, Z. Yu, S. Fan, Y. Cui, *Nano Lett.* 2010, **10**, 1979.

[28] M. G. Moharam, E. B. Grann, D.A. Pommet, T. K. Gaylord, *J. Opt. Soc. Am. A,* 1995, **12**, 1068.

[29] J. Gjessing, E. S. Marstein, A. Sudbø, *Opt. express,* 2010, **18**, 5481.

[30] D. Madzharov, R. Dewan, D. Knipp, *Opt. express,* 2011, **19**, 95.

[31] Diffractive optics: design, fabrication, and test (Ed: T. J. Suleski), Spie Press, 2004.

[32] R. Dewan, M. Marinkovic, R. Noriega, S. Phadke, A. Salleo, D. Knipp, *Opt. Express,* 2009, **17**, 23058.

[33] G. E. Jellison Jr, F. A. Modine, *Appl. Phys. Lett.,* 1996, **69**, 371.

[34] H. Yoshikawa, S. Adachi, *Jap. J. Appl. Phys.,* 1997, **36,** 6237.

[35] V. E. Ferry, L. A. Sweatlock, D. Pacifici, H. A. Atwater. *Nano Lett.,* 2008, **8**, 4391.

[36] V. E. Ferry, A. Polman, H. A. Atwater, *ACS nano,* 2011, **5**, 10055.

[37] C. Rockstuhl, F. Lederer, K. Bittkau, R. Carius, *Appl. Phys. Lett.,* 2007, **91**, 171104.

[38] M. Python, O. Madani, D. Dominé, F. Meillaud, E. Vallat-Sauvain, C. Ballif, *Sol. Energy Mater. Sol. Cells,* 2009, **93**, 1714.

[39] J. Bailat, D. Dominé, R. Schlüchter, J. Steinhauser, S. Faÿ, F. Freitas, C. Bücher, L. Feitknecht, X. Niquille, T. Tscharner, A. Shah, C. Ballif, *Proceedings of the 4th World WCPEC*, 2006, 1533–1536.